



Spectral wave flow attenuation within submerged canopies: Implications for wave energy dissipation

Ryan J. Lowe,¹ James L. Falter,² Jeffrey R. Koseff,³ Stephen G. Monismith,³ and Marlin J. Atkinson²

Received 26 March 2006; revised 16 August 2006; accepted 25 October 2006; published 11 May 2007.

[1] Communities of benthic organisms can form very rough surfaces (canopies) on the seafloor. Previous studies have shown that an oscillatory flow induced by monochromatic surface waves will drive more flow inside a canopy than a comparable unidirectional current. This paper builds on these previous studies by investigating how wave energy is attenuated within canopies under spectral wave conditions, or random wave fields defined by many frequencies. A theoretical model is first developed to predict how flow attenuation within a canopy varies among the different wave components and predicts that shorter-period components will generally be more effective at driving flow within a canopy than longer-period components. To investigate the model performance, a field experiment was conducted on a shallow reef flat in which flow was measured both inside and above a model canopy array. Results confirm that longer-period components in the spectrum are significantly more attenuated than shorter-period components, in good agreement with the model prediction. This paper concludes by showing that the rate at which wave energy is dissipated by a canopy is closely linked to the flow structure within the canopy. Under spectral wave conditions, wave energy within a model canopy array is dissipated at a greater rate among the shorter-period wave components. These observations are consistent with previous observations of how wave energy is dissipated by the bottom roughness of a coral reef.

Citation: Lowe, R. J., J. L. Falter, J. R. Koseff, S. G. Monismith, and M. J. Atkinson (2007), Spectral wave flow attenuation within submerged canopies: Implications for wave energy dissipation, *J. Geophys. Res.*, 112, C05018, doi:10.1029/2006JC003605.

1. Introduction

[2] Dissipation due to bottom friction is an important mechanism affecting the propagation and transformation of surface waves in nearshore environments, especially when the morphology of the benthos is considered hydraulically “rough.” Through dimensional arguments, *Jonsson* [1966] proposed that wave friction factors, which relate maximum bed stresses and rates of wave energy dissipation to near-bottom orbital velocities, depend on the ratio of the horizontal wave excursion amplitude A_∞ to some roughness length scale k_w . Numerous experiments conducted in the following decades confirmed this assertion, producing robust empirical relationships capable of relating wave friction factors for rough bottoms to this dimensionless ratio, A_∞/k_w [*Madsen*, 1994; *Nielsen*, 1992; *Swart*, 1974].

[3] *Dalrymple et al.* [1984] provided an alternative approach to modeling the dissipation of wave energy over very rough surfaces, termed “canopies,” by calculating the work done by a wave-driven flow on an idealized canopy formed by an array of vertical cylinders. Their model could be used to derive wave friction coefficients on the basis of simple geometric properties of a canopy, thereby linking large-scale dissipation of wave energy directly to small-scale flow interactions with individual canopy elements. A key assumption in their model, however, was that the local velocity field within a submerged canopy was equal to the free-stream velocity above the canopy. Moreover, the *Dalrymple et al.* [1984] formulation predicts that the wave friction coefficient depends only on the canopy geometry and is thus independent of the wave conditions (i.e., independent of A_∞/k_w). This assumption contradicts decades of studies on wave dissipation over rough surfaces, including measurements through vegetated canopies [e.g., *Dubi and Torum*, 1997]. As a consequence, *Mendez and Losada* [2004] later modified the *Dalrymple et al.* [1984] model by forcing the drag coefficient in the model to be a function of A_∞/k_w , where in their study k_w was taken as the canopy element diameter. However, other than producing good agreement between the predicted and observed dissipation for this data set, no physical explanation was offered

¹School of Environmental Systems Engineering, University of Western Australia, Crawley, Western Australia, Australia.

²Hawaii Institute of Marine Biology, University of Hawaii, Kaneohe, Hawaii, USA.

³Environmental Fluid Mechanics Laboratory, Department of Civil and Environmental Engineering, Stanford University, Stanford, California, USA.

for why the drag coefficient should depend so strongly on A_∞/k_w .

[4] Recently, *Lowe et al.* [2005b] (hereinafter referred to as LKM) conducted laboratory experiments and developed an analytical model to investigate the flow structure induced inside a submerged canopy by wave-driven oscillatory flow. Their model was developed by considering the momentum balance around individual canopy elements within a larger canopy, which for their case was constructed from an array of staggered circular cylinders. LKM demonstrated that flow inside a canopy was always less than above the canopy, and that the degree of flow attenuation varied as a function of canopy geometry parameters, for example, the height and spacing of the elements, as well as coefficients that parameterize the effects of various forces exerted by the canopy elements. LKM further showed that A_∞ was the single relevant wave parameter affecting the attenuation of flow inside the canopy, and identified three flow regimes governing the balance of momentum within a canopy: (1) one in which A_∞ was sufficiently small such that inertial forces dominate flow attenuation, resulting in the minimum attenuation of flow inside the canopy; (2) another where A_∞ was sufficiently large (i.e., quasi-unidirectional) such that the shear stress at the top of the canopy balances the canopy drag force, resulting in the maximum attenuation of the in-canopy flow; and (3) a final regime in which canopy drag, inertial and shear forces all made significant contributions to the momentum balance, leading to intermediate attenuation of the canopy flow.

[5] The attenuation of flow inside canopies is an important aspect of canopy flows which, to the best of our knowledge, has not yet been incorporated into prior models of dissipation by rough surfaces (canopies). We hypothesize that if dissipation of wave energy by canopies occurs mostly through interactions of the in-canopy flow with individual canopy elements, then the dynamics controlling the attenuation of flow inside a canopy will ultimately control the rate at which wave energy is dissipated. In order to test this hypothesis, this paper has three objectives. The first objective is to validate the canopy flow model of LKM under conditions in which drag, inertial, and shear forces all make significant contributions to the momentum balance, conditions that LKM were unable to create experimentally. The second objective is to extend the monochromatic wave model developed in LKM to spectral wave flows and then to evaluate its performance using field observations of spectral wave flow attenuation within a canopy. This is to give the model greater utility, given that natural canopies are generally exposed to random wave fields composed of a continuous range of different frequencies. The final objective is to use the canopy flow model to investigate how wave energy is dissipated by submerged canopies, and to compare these results to previous observations of wave dissipation over coral reefs.

2. Spectral Wave Canopy Flows

[6] In LKM, theory describing oscillatory flow through a submerged canopy was developed on the basis of the assumption that the oscillatory flow field could be characterized by a single frequency f ; that is, it was monochromatic. Equation (18) in that paper, governing horizontal

momentum inside the canopy, was numerically solved to calculate a representative in-canopy velocity \hat{U}_w as a function of the imposed (above-canopy) wave velocity $U_{\infty,w}$ and a collection of canopy geometry parameters. Note that \hat{U}_w was defined as the spatially averaged flow velocity inside the canopy (i.e., the averaging volume excludes the solid canopy elements) and the overhat symbol will be similarly used throughout this manuscript to refer to variables spatially averaged over the canopy fluid volume. Specifically, the governing canopy flow equation (now repeated here) was

$$\frac{d(\hat{U}_w - U_{\infty,w})}{dt} = \frac{|U_{\infty,w}|U_{\infty,w}}{L_s} - \frac{|\hat{U}_w|\hat{U}_w}{L_d} - \left(\frac{C_M \lambda_p}{1 - \lambda_p}\right) \frac{d\hat{U}_w}{dt}, \quad (1)$$

where L_s is a canopy shear length scale defined as

$$L_s = \frac{2h_c}{C_f} \quad (2)$$

and L_d is a canopy drag length scale defined as

$$L_d = \frac{2h_c(1 - \lambda_p)}{C_d \lambda_f}. \quad (3)$$

Here h_c is the canopy height and C_f , C_d and C_M are the empirical canopy friction, drag and inertia coefficients, respectively. The ‘‘lambda parameters’’ λ_f and λ_p in equation (1) were defined as

$$\lambda_f = A_f/A_T, \quad (4)$$

$$\lambda_p = A_p/A_T, \quad (5)$$

where A_f is the canopy element frontal area, A_p is the canopy element plan area, and A_T is the underlying surface area (total area divided by the number of elements). In both the work of LKM and in this present study, the canopies used for the experiments were constructed using an array of circular cylinders having diameter d and spacing S , such that $\lambda_f = h_c d / (S + d)^2$ and $\lambda_p = (\pi d^2 / 4) / (S + d)^2$. It is important to note equation (1) was originally developed for oscillatory flow where the free stream velocity was defined as

$$U_{\infty,w}(t) = U_{\infty,w}^{\max} \cos\left(\frac{2\pi t}{T}\right), \quad (6)$$

where $U_{\infty,w}^{\max}$ is the velocity amplitude and T is the period. The oscillatory velocity field given by equation (6) is notably both uniform over the water column (i.e., independent of z) and assumes no horizontal velocity gradients exist (i.e., convective accelerations $\partial U_{\infty,w} / \partial x$ are zero), so to apply equation (1) to surface wave conditions, the following two conditions must be satisfied. First, for surface waves the ratio of the convective acceleration $\partial U_{\infty,w} / \partial x$ to local acceleration must be small, which *Trowbridge and Madsen* [1984] showed scales as $O(kA_\infty)$ where k is the wave number. In most cases, $kA_\infty \ll 1$ such

that the effect of this nonlinear convective term can be neglected (e.g., for the wave conditions described in the field experiment below, $ka_\infty \sim O(0.01)$). Second, in the general case where surface waves are not shallow, the potential wave velocity amplitude $U_{\infty,w}^{\max}$ is not uniform over the water depth, as assumed in equation (6), and instead decreases below the free surface. However, LKM showed that for cases where kh_c is small (i.e., when the wave length is much greater than the canopy height), the wave velocity amplitude is roughly uniform over the depth of the canopy such that the wave forcing can be accurately approximated using equation (6) if $U_{\infty,w}^{\max}$ is taken as the velocity measured directly above the canopy (see section 2.2 in LKM for a discussion of this issue). For submerged canopies that occupy a small fraction of the water depth this condition is generally satisfied (e.g., for the canopy and wave conditions described in the field experiment below, $kh_c \sim O(0.01)$).

[7] To predict the in-canopy velocity \hat{U}_w , LKM numerically solved equation (1) using the forcing provided by equation (6), to calculate an attenuation parameter α_w defined as,

$$\alpha_w = \frac{\hat{U}_w^{rms}}{U_{\infty,w}^{rms}}, \quad (7)$$

where \hat{U}_w^{rms} and $U_{\infty,w}^{rms}$ are the root-mean-squared (rms) values of \hat{U}_w and $U_{\infty,w}$, respectively. Physically, the parameter α_w provides a measure of the reduction of the in-canopy flow from its above-canopy potential flow value; it thus takes a value $\alpha_w \approx 1$ (low attenuation) when flow within the canopy region is negligibly influenced by the presence of the canopy elements and a value $\alpha_w \approx 0$ (high attenuation) when minimal flow passes through the canopy.

[8] Under spectral wave conditions, wave velocities are characterized by the wave energy spectral density $S_U(f)$, which in practice is calculated in its discrete form $S_{U,j}(f_j)$, where the subscript j denotes the frequency component index. Note that for simplicity this analysis assumes that all of the wave energy propagates in the same direction (i.e., the spectrum is one-dimensional), which is often a good assumption in many shallow sites, including the field site chosen for the experiments discussed in section 3. A goal of the present study is to model how the imposed wave velocity spectrum $S_{U,j}$ above a canopy is attenuated inside the canopy among the different frequency components. The resulting spectrum inside the canopy, which will be denoted $\hat{S}_{U,j}$, can then be used to define a frequency-dependent attenuation parameter $\alpha_{w,j}$, analogous to α_w in equation (7). Since wave energy is proportional to velocity squared, in order for $\alpha_{w,j}$ to be consistent with equation (7), it is defined as

$$\alpha_{w,j} = \left(\frac{\hat{S}_{U,j}}{S_{U,j}} \right)^{1/2}. \quad (8)$$

It is worth noting that it may be tempting to apply the monochromatic model developed in LKM to determine $\alpha_{w,j}$ by simply applying the monochromatic model to each frequency component independently. While this would be permissible if the governing equation was linear, equation (1) is inherently nonlinear owing to the quadratic drag and shear stress terms. However, in the case discussed below

where the wave energy is concentrated in a relatively narrow frequency band, the monochromatic canopy flow model can be used to deduce a good estimate of the total attenuation of the in-canopy flow.

[9] A modeling approach is now developed to predict $\alpha_{w,j}$, given an above-canopy flow condition and the geometry of a canopy. To model the in-canopy flow under spectral wave conditions, we start by simulating a random time series $U_{\infty,w}(t)$ based on a specified wave spectrum S_U . To achieve this, we use the freely distributed Matlab toolbox Wave Analysis for Fatigue and Oceanography (WAFO) [Brodtkorb et al., 2000], although another random wave generator could alternatively have been used. For a given canopy having known geometry properties (i.e., L_s , L_d , C_M and λ_p), the simulated time series $U_{\infty,w}(t)$ is used as input into equation (1) and is numerically solved to generate a time series $\hat{U}_w(t)$ of the in-canopy flow (for a detailed description of this numerical technique see Appendix A). Finally, this in-canopy velocity time series $\hat{U}_w(t)$ is used to calculate the in-canopy wave spectrum $\hat{S}_{U,j}$ and $\alpha_{w,j}$ is calculated using equation (8).

[10] To demonstrate the application of the model and to introduce important features of spectral wave canopy flows, an example is first considered where the wave spectrum has a uniform distribution of the form

$$S_U = \begin{cases} S_O & 0 < f < 1\text{Hz} \\ 0 & \text{otherwise.} \end{cases} \quad (9)$$

While this distribution is strictly theoretical, it provides a useful demonstration of how wave energy is attenuated among different frequency components. For spectral waves, the rms wave velocity $U_{\infty,w}^{rms}$ is obtained by integrating the wave spectrum according to [Massel, 1996]

$$U_{\infty,w}^{rms} = \sqrt{2 \int_0^\infty S_U df}. \quad (10)$$

Substituting the form of S_U given in equation (9) into equation (10) shows that S_O (in units of m^2/s) is directly related to $U_{\infty,w}^{rms}$ (in units of m/s) by

$$S_O = \frac{\left(U_{\infty,w}^{rms} \right)^2}{2\text{Hz}}. \quad (11)$$

For a specified value of $U_{\infty,w}^{rms}$, the calculated spectrum $S_{U,j}$ given in equation (9) was input into the WAFO Matlab toolbox using the function “spec2sdat.m,” which simulated a 5000 second velocity time series using a 0.1 s time step. Note that for these simulations the canopy is defined such that it has identical properties to the cylinder array used for the experiment in section 3. Figure 1a shows a short segment of this time series for the case where $U_{\infty,w}^{rms} = 1\text{m/s}$. This time series then served as the input forcing for equation (1), and the initial value problem was numerically solved to simulate a time series of the in-canopy velocity $\hat{U}_w(t)$ (Figure 1b). With $\hat{U}_w(t)$, the WAFO function “dat2spec2.m” was used to calculate the in-canopy spectra $\hat{S}_{U,j}$. Given the random nature of $\hat{U}_w(t)$, this calculated $\hat{S}_{U,j}$ represents only one statistical estimate of the actual in-canopy spectrum, so this procedure was repeated

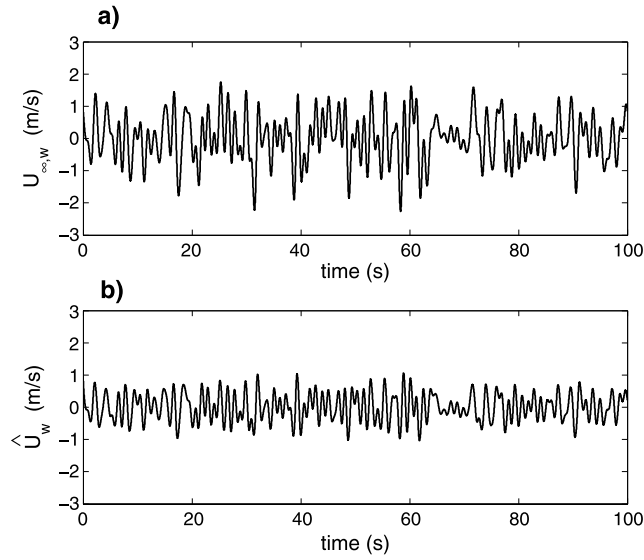


Figure 1. (a) Example time series $U_{\infty,w}(t)$ generated from the spectrum S_U defined in equations (9)–(11) for $U_{\infty,w}^{rms} = 1$ m/s. (b) The corresponding in-canopy velocity time series \hat{U}_w derived from the canopy flow model based on equation (1).

1000 times and the resulting spectra were averaged.

[11] For this example four different simulations were conducted, each defined according to equation (9), but using four different values of $U_{\infty,w}^{rms}$: 0.01, 0.1, 1 and 10 m/s. For each of these cases, $\alpha_{w,j}$ is plotted in Figure 2. These curves exhibit two important features of spectral wave canopy flows. First, for each value of $U_{\infty,w}^{rms}$, Figure 2 predicts that $\alpha_{w,j}$ will decrease as the period $T_j = 1/f_j$ of the component increases. Second, the curves in Figure 2 reveal that increasing the total flow energy (i.e., increasing S_O by increasing $U_{\infty,w}^{rms}$) will also cause the in-canopy flow to become more attenuated across all frequency components. Note that for monochromatic waves LKM showed that the attenuation parameter α_w is bounded by a maximum inertial-force-dominated value α_i (given by equation (24) in LKM), and a minimum unidirectional flow value α_c (given by equation (26) in LKM). In this example, for all frequency components considered, $\alpha_{w,j}$ falls between these limiting values $\alpha_c = 0.15$ and $\alpha_i = 0.77$.

[12] In physical terms, the dependency of $\alpha_{w,j}$ on both the wave period and velocity of the component can be explained in terms of the effect these parameters have on the momentum balance within the canopy. For oscillatory flows, the horizontal pressure gradient $\partial P_w/\partial x$ responsible for driving flow within a canopy is expressed in the second term on the left side of equation (1), since it is directly proportional to $\partial U_{\infty,w}/\partial t$. If we first consider $U_{\infty,w}(t)$ to have the monochromatic form given by equation (6), then $\partial P_w/\partial x \sim U_{\infty,w}^{max}/T$. However, according to equation (1), the canopy drag forces that attenuate the flow are governed by a quadratic drag law based on the in-canopy velocity \hat{U}_w , such that the drag force is proportional to $(\alpha_w U_{\infty,w}^{max})^2$. If we assume that the oscillatory pressure gradient is balanced by this canopy drag force then $\alpha_w \sim 1/(U_{\infty,w}^{max} T)^{1/2}$, revealing that the in-canopy will become more attenuated as either

$U_{\infty,w}^{max}$ or T increases, or equivalently as the horizontal wave excursion amplitude A_{∞} increases given that $A_{\infty} \sim U_{\infty,w}^{max} T$.

[13] For spectral wave conditions, the velocity field is better characterized in the frequency domain by the wave velocity spectrum $S_{U,j}$. Horizontal wave orbital excursion motions for spectral wave conditions are likewise described by the wave orbital excursion spectrum $S_{A,j}$, which is related to $S_{U,j}$ by [e.g., Madsen *et al.*, 1988]

$$S_{A,j} = \frac{S_{U,j}}{\omega_j^2} = \frac{S_{U,j} T_j^2}{(2\pi)^2}. \quad (12)$$

Thus, drawing an analogy to monochromatic waves where α_w decreases as the wave excursion length A_{∞} increases, for spectral waves the attenuation parameter $\alpha_{w,j}$ of frequency component j will likewise decrease as the spectral density $S_{A,j}$ of the wave orbital excursion increases. This is demonstrated in Figure 2, which shows that as $S_{A,j}$ is increased, either by increasing $S_{U,j}$ or T_j via equation (12), the in-canopy flow associated with that wave component is reduced.

3. Experimental Setup

[14] A field experiment was conducted using an array of the same plastic cylinders described in LKM. Each cylinder had height $h_c = 10$ cm and diameter $d = 5$ cm and was mounted on a 2.4 m \times 1.2 m sheet of plywood in a staggered array with a cylinder spacing $S = 7.5$ cm (Figure 3a). In their laboratory experiments, LKM used spacings $S = 5.0, 10.0,$ and 15.0 cm, such that the spacing used for this field study fall within the range used in the laboratory experiments. Note that a spacing $S = 7.5$ cm was specifically chosen for

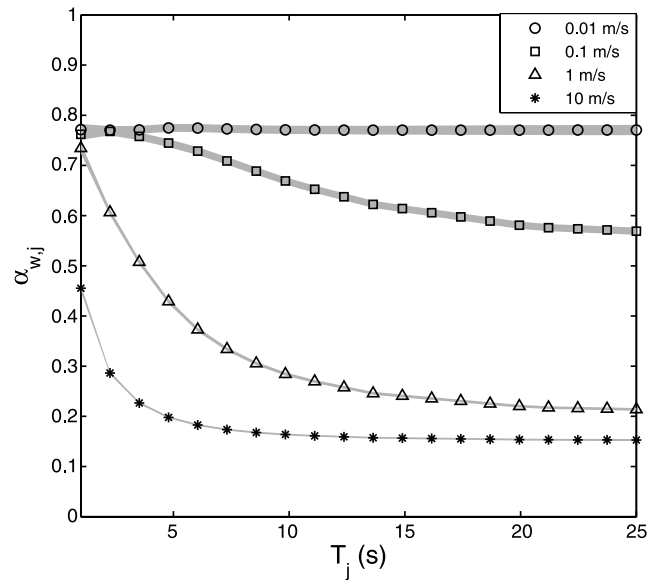


Figure 2. Parameter $\alpha_{w,j}$ calculated as a function of the period T_j of the wave component, as predicted using the model for a uniform spectrum given by equations (9)–(11). Simulations were run for $U_{\infty,w}^{rms} = 0.01, 0.1, 1,$ and 10 m/s. Shaded regions denote the 95% confidence intervals of the simulations.

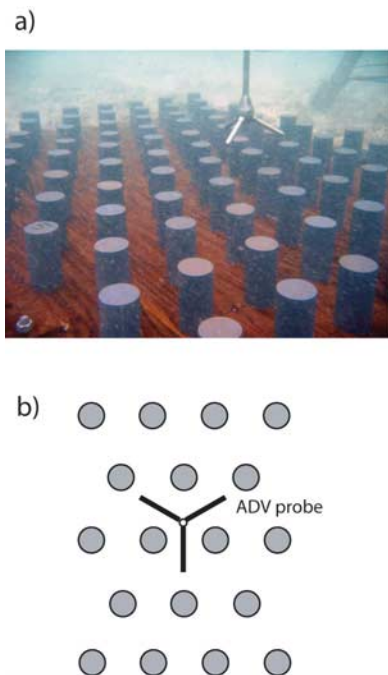


Figure 3. (a) Photograph of the model canopy at the field site and the lower acoustic Doppler velocimeter (ADV) used to measure the velocity inside the canopy. The ADV sample volume was 15 cm below the probe at the midheight of the canopy. (b) Diagram illustrating how the ADV probe was oriented to sample between the cylinders.

this field study because it was the densest spacing that would permit measurement of the flow inside the canopy using the type of acoustic Doppler velocimeter (ADV) that we had (see below). Given these geometry parameters, the lambda parameters for the field canopy, calculated using equations (4) and (5), were $\lambda_f = 0.32$ and $\lambda_p = 0.13$.

[15] The experiment was conducted on the reef flat region of the Kaneohe Bay barrier reef, Oahu, Hawaii (21°29'N, 157°48'W). For a detailed description of the field site, refer to *Lowe et al.* [2005a]. To ensure that the plywood sheet would lie flat on the seafloor, a site was chosen that had a very flat limestone foundation, yet was covered by a thin (~2 cm thick) layer of sand. Waves on the Kaneohe reef flat propagate in a highly predictable direction set by the shallow reef bathymetry [*Lowe et al.*, 2005a], hence making the 1-D wave assumption discussed in section 2 valid at this site. The plywood sheet was arranged such that its lengthwise direction was oriented into the wave direction (~225°). In order for the canopy flow to sufficiently develop, it is important that the cylinder array be sufficiently large to ensure that edge effects can be ignored. As discussed in section 2, the wave parameter that determines the canopy flow attenuation is the horizontal wave orbital excursion length. For random waves a wave excursion length A_{∞}^R can be defined on the basis of a representative period T^R and velocity $U_{\infty,w}^R$ (see section 4 for definitions), according to $A_{\infty}^R = U_{\infty,w}^R T^R / (2\pi)$ [*Madsen*, 1994]. A_{∞}^R was calculated to be 28 cm during the experiment, much smaller than the 2.4 m length of the cylinder array, so the in-canopy

velocities measured near the center of the canopy can be assumed to be fully developed.

[16] A sawhorse instrument frame straddled the cylinder array and supported two Nortek Vector ADVs (Figure 3a), which measured velocities at roughly the center of the array. Both ADVs were cabled to a laptop computer located on a boat anchored near the site. The upper ADV sampled at a height $z = 60$ cm above the plywood base (located at $z = 0$ cm). The lower ADV sampled within the cylinder array at the midcylinder height ($z = 5$ cm), and the ADV probe was carefully oriented such that its three acoustic beams fit between the cylinders with no interference (Figure 3b). Note that the velocity \hat{U}_w in equation (1) is the spatially averaged in-canopy velocity, while the velocity measured in the experiment is at a single midcanopy height location. LKM showed that under wavy conditions, the in-canopy flow is mostly uniform throughout the canopy such that the velocity measured at this midcanopy height is expected to well-approximate this spatially averaged velocity. During the experiment, the ADVs each sampled velocity and pressure synchronously at 16 Hz for 2 hours. Over this time, the tide was rising such that the depth h varied between 1.5 m and 1.8 m. Time-averaged current speeds were measured to be very weak during the experiment (<2 cm/s), such that the near-bottom flow was effectively dominated by wave-orbital motion.

4. Measurement and Prediction of the Spectral Wave In-Canopy Flow

[17] The complete ADV time series was divided into twelve, 10-min records, each having 9600 velocity samples. For general wave-current flows, the instantaneous velocity u can be decomposed as

$$u = U_c + U_w + u', \quad (13)$$

where U_c is the steady velocity associated with the current, U_w is the unsteady wave motion, and u' is the turbulent velocity. To compare the attenuation of wave energy within the canopy we should therefore remove the effect of turbulence, which is also an unsteady quantity. To achieve this, the linear filtration technique proposed by *Benilov and Filyushkin* [1970] was used, which treats the wave velocities as any unsteady velocity that is correlated with the free surface elevation (or in our case the instantaneous pressure P_w measured by the upper ADV). It should be noted that the residual, uncorrelated signal will be labeled “turbulence,” even though this signal may include both turbulence and noise effects, since both will be uncorrelated with the free surface elevation. Application of the Benilov filtration approach allows the measured instantaneous velocity spectrum S_u to be decomposed into a wave spectrum S_U and turbulence spectrum $S_{u'}$. As shown below, if it is assumed that the measured instantaneous spectrum S_u is equal to the wave spectrum S_U , some error can be introduced, particularly among the higher-frequency components where $S_{u'}$ can be a significant fraction of the total flow energy.

[18] For each 10-min record, the *Benilov and Filyushkin* [1970] method was used to decompose S_u into S_U and $S_{u'}$.

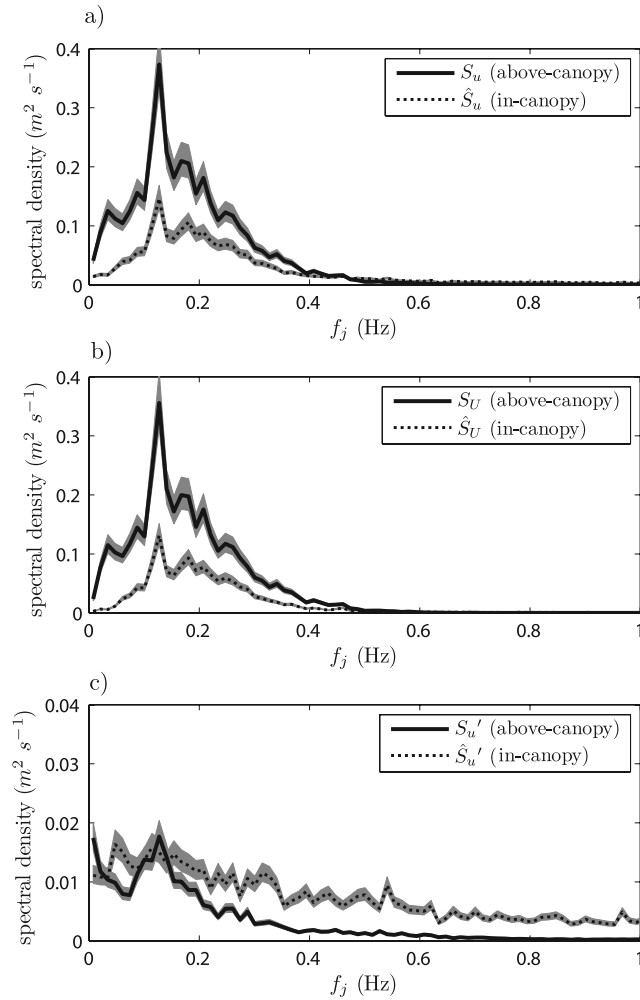


Figure 4. Decomposition of the spectrum measured above and within the canopy (shaded regions denote the 95% confidence intervals of the calculations). (a) Spectra derived from the original velocity time series. (b) The decomposed wave contribution. (c) The decomposed turbulence contribution (note the order of magnitude difference in the vertical scale).

Figure 4 shows the average spectra measured by the lower and upper ADVs, obtained by averaging all twelve individual spectra. For the upper ADV, virtually all of the energy S_u is due to the wave contribution S_U ; this is expected since turbulence levels should be relatively weak away from the canopy roughness. The resulting wave spectrum S_U shows a well-defined peak period of $T_p = 7.8$ s, and the spectrum gradually tapers below and above this period. Note that 95% of the wave energy is contained in the frequency range 0.04–0.5 Hz, so in the subsequent analysis we will focus on waves with periods between 2 and 25 s.

[19] Figure 4 shows that the equivalent spectra \hat{S}_U measured inside the canopy has noticeably different characteristics than the above-canopy spectrum S_U . First, the total wave energy measured inside the canopy is significantly reduced from the above canopy value. Second, turbulence levels are generally higher inside the canopy, as expected owing to the interaction of the flow with the cylinders. This causes the wave spectrum \hat{S}_U to be slightly reduced from the

spectrum \hat{S}_u . This difference between \hat{S}_U and \hat{S}_u is more significant in the high-frequency region, where very little wave energy exists such that turbulence levels become comparable to the wave energy.

[20] For non-shallow wave conditions, the magnitude of the wave orbital velocities will decay below the free surface at a rate that varies among the frequency components [Dean and Dalrymple, 1991]. To calculate $\alpha_{w,j}$, we are only interested in the attenuation resulting from the interaction of the oscillatory flow with the canopy elements, such that the effect of the vertical decay of the potential wave velocity field should be removed (note that this was also done for the monochromatic wave case in section 4.2 of LKM). As a result, a correction factor ϕ_j is calculated, which represents the ratio of the velocity predicted from linear wave theory for the upper ADV at height $z = d_{high}$, to the velocity predicted for the lower ADV at height $z = d_{low}$, for each

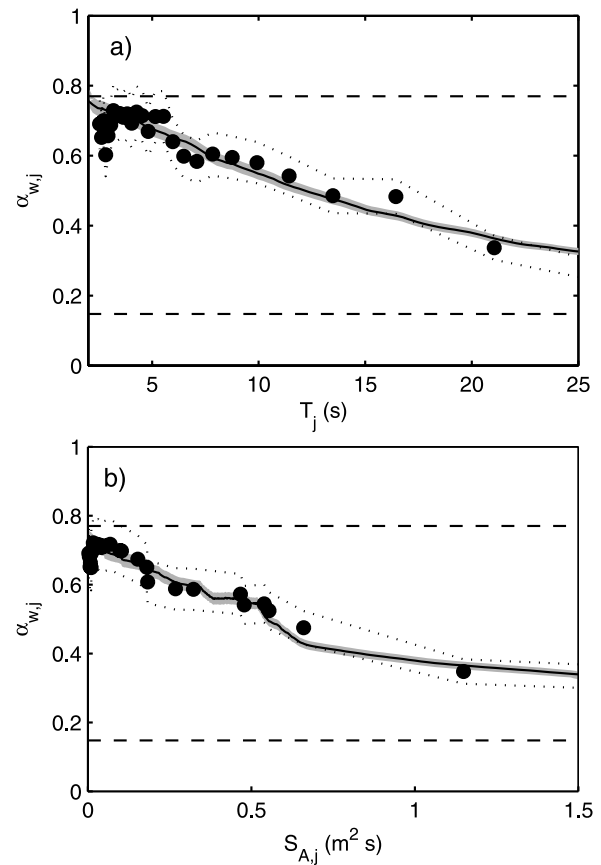


Figure 5. (a) Spectral wave attenuation parameter $\alpha_{w,j}$ as a function of the wave period T_j of the spectral component. (b) Same data plotted as a function of the spectral density of the wave orbital excursion length $S_{A,j}$. Circles denote field measurements, dotted lines denote the boundary of the 95% confidence limits of measured $\alpha_{w,j}$, solid lines denote predicted $\alpha_{w,j}$ calculated from the model using the measured wave spectrum S_U above the canopy as the model input (shaded region denotes the 95% confidence limits in the calculations), and dashed lines denote the unidirectional and inertial force dominated values for this canopy geometry, $\alpha_c = 0.15$ and $\alpha_i = 0.77$, respectively.

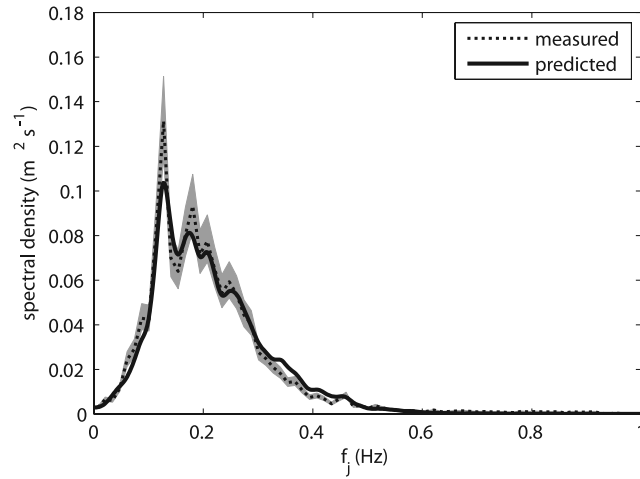


Figure 6. The dotted line denotes the measured in-canopy wave velocity spectrum \hat{S}_U (shaded region denotes the 95% confidence limits). The solid line denotes the predicted in-canopy spectrum \hat{S}_U obtained from the model using the above canopy spectrum S_U as input.

frequency component j ; that is [Dean and Dalrymple, 1991],

$$\phi_j = \frac{\cosh(k_j d_{\text{high}})}{\cosh(k_j d_{\text{low}})}, \quad (14)$$

where k_j is the wave number of the j th component. The spectral wave attenuation parameter was then calculated as

$$\alpha_{w,j} = \left(\phi_j^2 \frac{\hat{S}_{U,j}}{S_{U,j}} \right)^{1/2}, \quad (15)$$

where $\hat{S}_{U,j}$ and $S_{U,j}$ are the wave velocity spectra measured by the lower and upper ADVs, respectively. Note that ϕ_j was relatively small for all frequencies considered (i.e., at most ~ 1.1 at the highest frequency 0.5 Hz). Figure 5a shows that for short-period components, $\alpha_{w,j}$ attains a maximum value near 0.7 and gradually decreases with increasing wave period to a minimum value of roughly 0.3 for $T = 25$ s. The longest-period components are therefore more than twice as attenuated as the shorter-period components. More precisely, the theory developed in section 2 predicts that $\alpha_{w,j}$ will decrease as the spectral density of the wave-orbital excursion $S_{A,j}$ increases (Figure 5b) which generally corresponds to longer-period components (equation (12)).

[21] In order to test the ability of the model developed in section 2 to predict $\alpha_{w,j}$, the coefficients C_f , C_d and C_M that parameterize the various canopy forces in the model must first be specified. While values of C_d and C_M are well-established for infinitely long cylinders in isolation, little is known about how these coefficients are modified when cylinders reside inside a submerged canopy. In this case the cylinders are of finite length (thereby introducing three-dimensional flow effects) and any forces exerted on them may be influenced by the wakes generated from neighboring elements [Ghisalberti and Nepf, 2004]. Unfortunately,

general empirical formulas for C_d and C_M that incorporate these effects do not currently exist, which would need to be derived from data incorporating a wide variety of flow conditions and canopy geometries. However, given that the canopy used in this field experiment was constructed using the exact same canopy elements used in LKM, and also arranged to have a similar density, we therefore assume the same values for these coefficients (i.e., $C_f = 0.02$, $C_d = 2.5$, $C_M = 2.0$), which are based on the best data available in the literature for these particular cylinder arrays (see LKM, p. 8, for a discussion of this issue).

[22] To predict $\alpha_{w,j}$ the WAFO toolbox was used to simulate 1000 independent time series, each 5000 s long, on the basis of the input spectrum $S_{U,j}$. These time series served as the forcing for equation (1), and the initial value problem was numerically solved for each time series. This procedure generated a set of \hat{U}_w time series, which were converted to a set of in-canopy flow spectra $\hat{S}_{U,j}$ and were then averaged. Figure 6 shows the resulting $\hat{S}_{U,j}$ predicted by the model. This spectrum was used with equation (8) to calculate $\alpha_{w,j}$ (Figure 5). The model predicts that at $T = 2$ s, $\alpha_{w,j} \approx 0.75$ and decreases as the wave period increases to a minimum value $\alpha_{w,j} \approx 0.30$ at $T = 25$ s. The model result therefore agrees very well with measured $\alpha_{w,j}$, confirming that longer period waves are indeed significantly more attenuated than shorter-period motions. The close agreement with the observations also suggests that the values chosen in LKM for the empirical force coefficients ($C_f = 0.02$, $C_d = 2.5$ and $C_M = 2.0$) accurately predict flow attenuation for this canopy in the regime between the unidirectional and inertial force dominated limits where all canopy forces are important, which could not be tested in the laboratory experiments of LKM.

[23] Finally, we conclude our discussion of these experimental observations by investigating whether the much simpler monochromatic canopy flow model developed in LKM can provide a reasonable estimate of the attenuation of the total wave energy inside the canopy. This would be useful, for example, if only the rms velocity inside the canopy is required and not necessarily how the wave energy is distributed among the different frequency components. To make this comparison, we first must define representative velocities for the in-canopy and above-canopy flows, \hat{U}_w^R and $U_{\infty,w}^R$ respectively, as well as a representative wave frequency f^R . Following Madsen *et al.* [1988], we take these representative velocities to be the rms values, \hat{U}_w^{rms} and $U_{\infty,w}^{\text{rms}}$, respectively, and f^R to be the energy weighted-averaged frequency, defined by

$$f^R = \frac{\sum_{j=1}^N f_j S_{U,j}}{\sum_{j=1}^N S_{U,j}}, \quad (16)$$

which is related to a representative period by $T^R = 1/f^R$. Given $S_{U,j}$ measured in Figure 4, we find that $T^R = 5.7$ s for the above-canopy flow. The representative velocities for the measured above- and in-canopy flows, calculated using equation (10), are $U_{\infty,w}^{\text{rms}} = 31$ cm/s and $\hat{U}_w^{\text{rms}} = 19$ cm/s, respectively. The ratio of these two velocities can be used to define a representative value of the attenuation parameter

$\alpha_w^R = 0.62$. Therefore, to compare this observed attenuation with the value predicted from the monochromatic model in LKM, we assume that the imposed wave field is monochromatic having a velocity $U_{\infty,w}^{rms} = 31$ cm/s and period $T^R = 5.7$ s. Following the approach outlined in LKM, equation (1) is solved for this monochromatic condition giving 0.63, which agrees very well with $\alpha_w^R = 0.62$ measured. These results demonstrate that the monochromatic model can be used to accurately predict the attenuation of the total wave energy in a spectral wave flow, assuming that the wave conditions are similar to those encountered during experiment; that is for conditions where the wave energy is within a relatively narrow frequency band. However, this may not always be the case, for example, when wave conditions are derived from two or more energy sources having different dominant periods, causing the resulting spectrum to have multiple peaks.

5. Dissipation of Wave Energy by Canopies

[24] We now demonstrate how the rate at which wave energy is dissipated by a submerged canopy is closely linked to the in-canopy flow structure. Using results from the preceding flow attenuation study, we first investigate how wave energy is dissipated under monochromatic conditions and then expand the scope of the analysis to incorporate general spectral wave forcing.

5.1. Monochromatic Wave Dissipation

[25] The rate of dissipation per unit plan area ε of an oscillatory flow propagating over a rough surface is generally parameterized according to [e.g., *Jonsson, 1966*]

$$\varepsilon = \frac{2}{3\pi} \rho f_e \left(U_{\infty,w}^{\max} \right)^3, \quad (17)$$

where f_e is the wave energy dissipation factor and $U_{\infty,w}^{\max}$ is the maximum horizontal wave velocity above the roughness. To predict wave dissipation by canopies, *Dalrymple et al.* [1984] presented a simple model that could be used to calculate f_e by determining the rate of work done by the flow against the canopy drag forces. However, a key assumption in their approach when it is applied to submerged canopies, is that the local flow field inside a canopy is not modified by the presence of the canopy elements, which we have shown in the preceding sections is not the case. Therefore we present an alternative canopy dissipation model that explicitly accounts for the effect of this in-canopy flow attenuation.

[26] The average rate of dissipation by a canopy can be determined by first spatially averaging the conservation of energy equation over a control volume formed by a repeating canopy element, and then time-averaging over a wave period (details of the approach are presented in Appendix B). The resulting equation shows that wave dissipation is directly related to the rate of work done by the in-canopy flow against the forces exerted by the canopy elements. LKM showed that three canopy forces will act (i.e., shear, drag, and inertial) such that the total rate of dissipation within the canopy per unit plan area ε can be decomposed into its respective force contributions; that is,

$$\varepsilon = \varepsilon_s + \varepsilon_d + \varepsilon_i, \quad (18)$$

where ε_s , ε_d , and ε_i are the rates of dissipation due to shear at the top of the canopy, drag and inertial forces, respectively. In Appendix B each of these terms is evaluated, which are

$$\varepsilon_s = \frac{2}{3\pi} \rho C_f \left(U_{\infty,w}^{\max} \right)^3 \quad (19)$$

for the shear stress contribution,

$$\varepsilon_d = \frac{2}{3\pi} \rho C_d \lambda_f \alpha_w^3 \left(U_{\infty,w}^{\max} \right)^3 \quad (20)$$

for the drag contribution, and

$$\varepsilon_i = 0 \quad (21)$$

for the inertial contribution, owing to the inertial force and velocity being 90 degrees out of phase. Results from equations (19), (20), and (21) can then be substituted into equation (18) giving

$$\varepsilon = \frac{2}{3\pi} \rho \left[C_f + C_d \lambda_f \alpha_w^3 \right] \left(U_{\infty,w}^{\max} \right)^3. \quad (22)$$

Finally, comparison of equation (22) with equation (17) shows that the energy dissipation factor f_e for a canopy can be determined using the simple expression

$$f_e = C_f + C_d \lambda_f \alpha_w^3. \quad (23)$$

Equation (23) reveals that f_e will attain a minimum value $f_e = C_f$ when the in-canopy flow is weak (i.e., α_w is small), but increases as an increasing amount of flow passes through the canopy (i.e., as α_w increases).

[27] As an example application, we can use results from section 4 with equation (23) to calculate a value of f_e for the canopy used in the experiment. It was shown that if to an approximation the spectral wave field is treated as a monochromatic wave with all of its energy contained in the representative wave period T^R , then the representative value of α_w was 0.62. Substituting this into equation (23) gives $f_e = 0.21$, which is much greater than the canonical value of $f_e = O(0.001)$ associated with smooth beds [*Dronkers, 1964*]. This value is in fact quite similar to previous values of f_e cited for coral reefs, which have been obtained by measuring the decrease in wave energy flux across a section of reef, for example, $f_e = 0.28$ [*Gerritsen, 1981*], $f_e = 0.15$ [*Nelson, 1996*], $f_e = 0.22$ [*Falter et al., 2004*], and $f_e = 0.24$ [*Lowe et al., 2005a*].

[28] It should be emphasized that equation (23) is equivalent to the model by *Dalrymple et al.* [1984] if α_w is assumed to always equal one (i.e., that the in-canopy flow is not attenuated). Note that for $\alpha_w = 1$, equation (23) predicts that $f_e = 0.82$, which is 4 times greater than value obtained with flow attenuation accounted for. In addition, the model by *Dalrymple et al.* [1984] predicts that f_e for a given canopy will be constant under varying A_{∞} , a characteristic inconsistent with decades of studies on wave dissipation over rough bottoms (see *Nielsen [1992]* for a review) as well as for vegetated canopies [e.g., *Dubi and Torum,*

1997]. To incorporate this observed dependency of f_e on A_∞ , Mendez and Losada [2004] modified the model by Dalrymple et al. [1984] by replacing C_d with an empirical “modified” drag coefficient \tilde{C}_d that decreased as A_∞ is increased [i.e., see Mendez and Losada, 2004, Figure 4]. While Mendez and Losada [2004] showed that their approach could be used to accurately determine dissipation rates in canopies, \tilde{C}_d needed to be empirically corrected for each canopy and wave condition considered. Interestingly, for cases where canopy drag forces dominate, f_e in equation (23) is equivalent to C_d in the work of Mendez and Losada [2004], since both are used to parameterize wave dissipation as a function of the above-canopy wave condition; therefore equation (23) specifically predicts that \tilde{C}_d (or f_e) will scale as $C_d \lambda_f \alpha_w^3$. In both LKM and in the present study, it was found that α_w will decrease for a given canopy as the wave excursion length A_∞ is increased. Thus \tilde{C}_d (or f_e) should also decrease as A_∞ is increased, which is consistent with the observations of Mendez and Losada [2004]. Therefore, while the submerged canopies evaluated by Mendez and Losada [2004] are somewhat different from those used in the present study (i.e., most notably they are composed of flexible vegetation), our study provides a physical mechanism to explain why the dissipation of wave energy by a canopy becomes less efficient as A_∞ increases: a trend consistent with a majority of the prior literature on wave dissipation over rough bottoms.

5.2. Spectral Wave Dissipation

[29] Madsen et al. [1988] developed a model (later modified by Madsen [1994]) that could be used to predict dissipation of spectral wave energy by rough beds, on the basis of theory originally developed for monochromatic waves. This model has been used to predict spectral wave transformation in a number of near shore studies [e.g., Ardhuin et al., 2001] and has been found to accurately describe spectral wave dissipation in both laboratory and field studies [e.g., Lowe et al., 2005a; Mathisen and Madsen, 1999]. In this model, the spectral wave field is assumed to be characterized by a single representative velocity $U_{\infty,w}^R$, such that the frequency-dependent dissipation function $\varepsilon_{f,j}$ is modeled according to

$$\varepsilon_{f,j} = \frac{1}{4} \rho f_{e,j} U_{\infty,w}^R U_{\infty,j}^2, \quad (24)$$

where $f_{e,j}$ is the frequency-dependent energy dissipation factor and $U_{\infty,j}$ is the velocity amplitude associated with the j th frequency component. $U_{\infty,j}$ can be obtained from the wave velocity spectrum using

$$U_{\infty,j} = \sqrt{2S_{U_j} \Delta f_b}, \quad (25)$$

where Δf_b is the discrete frequency bandwidth. Importantly, equation (24) is compatible with equation (17), since for monochromatic waves (i.e., when $U_{\infty,j} = U_{\infty,w}^{\max}$) the appropriate representative velocity is $U_{\infty,w}^R = (8/3\pi)U_{\infty,w}^{\max}$ [Kajiura, 1968; see also Madsen et al., 1988]. For spectral wave conditions, following earlier work by Collins [1972], Madsen et al. [1988] showed that the relevant representative velocity is the root-mean-squared velocity; that is,

$$U_{\infty,w}^R = U_{\infty,w}^{\text{rms}}, \quad (26)$$

which can be computed using equation (10). Given an incident wave spectrum S_{U_j} , equation (24) can be used to calculate the dissipation function $\varepsilon_{f,j}$ if the energy dissipation factor $f_{e,j}$ is known. For monochromatic waves, an expression governing f_e was developed above, on the basis of properties of the canopy and the magnitude of the in-canopy oscillatory flow (see equation (23)). In Appendix C, an expression for $f_{e,j}$ associated with spectral waves is derived for use in equation (24), which gives,

$$f_{e,j} = C_f + C_d \lambda_f \alpha_w^R \alpha_w^2. \quad (27)$$

which is similar to equation (23). It is, however, a function of the frequency-dependent flow attenuation parameter $\alpha_{w,j}$ defined in equation (8) and a representative flow attenuation parameter α_w^R defined as the ratio of \hat{U}_w^{rms} and $U_{\infty,w}^{\text{rms}}$ (see Appendix C). Therefore equation (27) predicts that components of a spectral wave flow that can penetrate more readily into a canopy will be more efficient at dissipating their energy.

[30] Using results from section 4, we can apply equation (27) in conjunction with data from Figure 5 to estimate $f_{e,j}$ for this model canopy. The resulting $f_{e,j}$ plotted in Figure 7a varies from $f_{e,j} \approx 0.3$ for the $T = 2$ s component to $f_{e,j} \approx 0.1$ for the $T = 25$ s component, indicating that the wave energy will indeed be dissipated more efficiently among the shorter-period motions owing to the enhanced in-canopy flow they generate. This trend is quite similar to previous observations of spectral wave energy dissipation on the Kaneohe Bay reef flat measured over natural roughness by Lowe et al. [2005a]. The variation of wave dissipation among the wave components during this experiment was measured over a two-week period at the same location on the reef where the model canopy was located for the present study. During the experiment of Lowe et al. [2005a], the rms wave velocity was $U_{\infty,w}^{\text{rms}} = 27$ cm/s, which is very near the $U_{\infty,w}^{\text{rms}} = 31$ cm/s measured for this present experiment. Figure 7b shows that $f_{e,j}$ calculated for this natural reef roughness decreases as the period of the component increases, achieving its largest values $\approx 0.3 - 0.4$ among the shortest-period components and smallest values ≈ 0.1 among the longest-period motions (Figure 7b). This supports the notion that wave energy is dissipated more efficiently by the reef among the shorter-period components since these motions more readily penetrate into the roughness features on the reef flat. Moreover, the shape of $f_{e,j}$ measured on the reef is itself remarkably similar to the $f_{e,j}$ curve for the model canopies in Figure 7a, despite the fact that the geometry of the coral roughness is much more complex than a simple cylinder array. Given that the wave conditions were roughly the same between experiments, the close agreement between Figure 7a and 7b may suggest that wave energy is dissipated on the reef by roughness features having length scales similar to that of the model canopy. In fact, the hydraulic roughness length k_w of the reef flat measured by Lowe et al. [2005a] was 16 cm, which is comparable to the 10 cm height and 7.5 cm spacing of the cylinders.

6. Summary and Conclusions

[31] By building on ideas originally developed in LKM for monochromatic waves, a modeling approach was

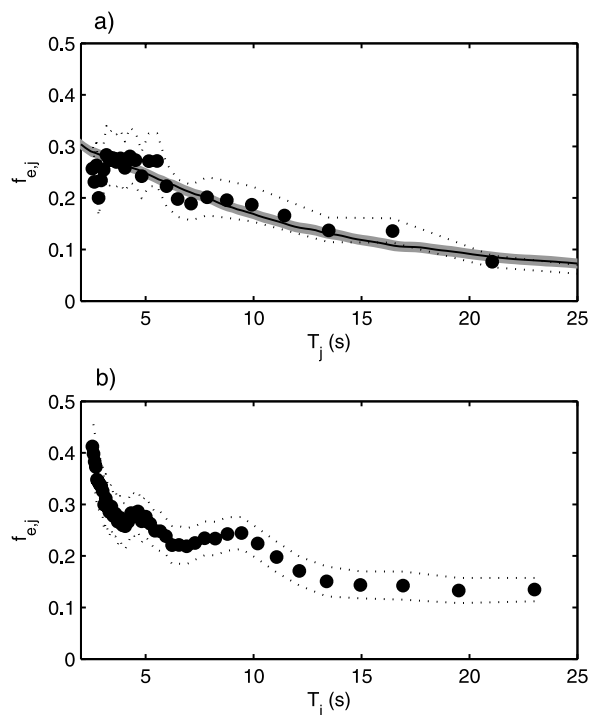


Figure 7. (a) Energy dissipation factor $f_{e,j}$ for the model canopy obtained using the data in Figure 5a with equation (27), as a function of the period of the spectral component T_j . Circles denote the result based on the field measurements. Dotted lines denote the boundary of the 95% confidence limits for the measurements. Solid lines denote the predicted $f_{e,j}$ from the model simulation (shaded region denotes the 95% limits of the calculation). (b) Energy dissipation factor $f_{e,j}$ measured on the Kaneohe Bay barrier reef as a function of the period of the spectral component (dotted lines denote the 95% confidence intervals). The data points were obtained by averaging the measured $f_{e,j}$ between the three pairs of sites shown in Figure 13 of *Lowe et al.* [2005a]. Note the qualitative similarity between the two figures.

developed in section 2 to predict how a spectral wave flow is attenuated within a submerged canopy. The theory predicts that the flow will be attenuated differently among the spectral components, with greater flow occurring among the components that have smaller orbital excursion lengths; these components generally correspond to the shorter-period wave motions. To investigate the model performance, a field experiment was conducted using the same model canopies used in the laboratory study of LKM. Results confirmed that shorter-period wave motions can indeed penetrate more readily into a canopy, and the model was shown to accurately predict the spectral distribution of flow attenuation. This close agreement between the model prediction and the observations not only has implications for the present study, but also for the monochromatic wave study of LKM. A shortcoming of the work by LKM was that the flume used in their study could only verify the model performance under a very limited range of wave conditions. By conducting experiments in the field during

the present study, where the waves were larger and their energy was distributed over a broad range of frequencies, the general theory behind the LKM model was effectively tested over a wide range of different wave conditions. Given that both the spectral model and the monochromatic LKM model are governed by the same equation, the close agreement between the field observations and model predictions suggests that equation (1) properly captures the physics responsible for wave attenuation within submerged canopies, and moreover suggests that the values specified for the empirical coefficients C_f , C_d , and C_M correctly parameterize the effect of the force terms for this canopy.

[32] Section 5 focused on the issue of wave energy dissipation by canopies, and showed that the rate of dissipation is governed by the in-canopy flow structure, thereby linking large-scale dissipation to in-canopy flow mechanics. A model for monochromatic wave dissipation was first presented, which predicts that rates of wave dissipation will increase as increasing flow passes through a canopy, that is, as α_w increases. Following *Madsen et al.* [1988], an analogous spectral wave dissipation model was developed, which predicts that dissipation will be higher among wave components that more readily pass into the canopy, that is, those components having higher $\alpha_{w,j}$. Results from the first part of the paper revealed that as the orbital excursion length A_∞ of a wave (or wave component) is increased, the flow inside a canopy will become increasingly attenuated. Therefore dissipation of wave energy by canopies, or more specifically the energy dissipation factor f_e , will generally be a strong function of A_∞ . This result is consistent with several decades of empirical studies on wave-energy dissipation over rough bottoms.

[33] In order to apply the models (of both flow and dissipation) to arbitrary canopies, the primary challenge remains choosing appropriate values for the coefficients used to parameterize the canopy force terms. Even for the simplest case where the canopy is formed using a cylinder array, the issue is still not straightforward. Natural canopies formed by benthic organisms are further complicated by the complex geometries these organisms form. Typically, these canopies are inhomogeneous (e.g., the coral community in Figure 1a of LKM) and in some cases may be flexible (e.g., for canopies formed by sea grass or macroalgae). The models proposed above could be extended to incorporate such effects, however, additional data must first be collected to provide appropriate values for the empirical canopy force coefficients. For inhomogeneous canopies experiencing unidirectional flow, *Coccal and Belcher* [2005] proposed to define the geometry on the basis of weighted-averaged properties of the entire canopy. A further complication for modeling flow and dissipation within flexible canopies is that the canopy may change its geometry (and hence resistance properties) as the flow conditions change. For example, sea grass blades may increasingly deflect into a unidirectional flow as the flow speed increases. Furthermore, under wave conditions a flexible canopy may also change its geometry considerably over a wave period, thereby altering the drag and inertial forces the canopy elements experience. Some studies have proposed using modified force coefficients to incorporate this effect [e.g., *Denny and Gaylord*, 2002], and similar formulations could eventually be included in the models proposed above.

Therefore this present study can be viewed as a first step toward developing a mechanistic model of how a wave-driven flow is attenuated and dissipated within submerged canopies. Future versions of the present model could be modified to include the complicating effects associated with flexibility and canopy inhomogeneity, when additional experimental data becomes available.

Appendix A: Numerical Solution of the Canopy Flow Equation Under Spectral Wave Conditions

[34] A model was developed in section 2 to predict the wave spectrum \hat{S}_U inside a canopy, given geometric properties of a canopy and the wave spectrum S_U above the canopy. This model relies on the numerical solution of equation (1) using the time series of $U_{\infty,w}(t)$ output from the WAFO toolbox. Equation (1) is first rearranged as

$$(1 + C) \frac{d\hat{U}_w}{dt} = \frac{|U_{\infty,w}|U_{\infty,w}}{L_s} - \frac{|\hat{U}_w|\hat{U}_w}{L_d} + \frac{dU_{\infty,w}}{dt}, \quad (\text{A1})$$

where

$$C = \frac{C_M \lambda_p}{1 - \lambda_p}. \quad (\text{A2})$$

Equation (A1) is then discretized using forward differencing according to

$$(1 + C) \left[\frac{\hat{U}_w^{(i+1)} - \hat{U}_w^{(i)}}{\Delta t} \right] = \frac{|U_{\infty,w}^{(i)}|U_{\infty,w}^{(i+1)}}{L_s} - \frac{|\hat{U}_w^{(i)}|\hat{U}_w^{(i+1)}}{L_d} + \frac{dU_{\infty,w}^{(i)}}{dt}, \quad (\text{A3})$$

where the nonlinear terms are linearized by staggering the time steps. Finally, equation (A3) can be rearranged to give

$$\hat{U}_w^{(i+1)} = \frac{1}{D} \left[(1 + C) \hat{U}_w^{(i)} + \frac{|U_{\infty,w}^{(i)}|U_{\infty,w}^{(i+1)}}{L_s} + \frac{dU_{\infty,w}^{(i)}}{dt} \right], \quad (\text{A4})$$

where

$$D = \frac{(1 + C)}{\Delta t} + \frac{|\hat{U}_w^{(i)}|}{L_d}. \quad (\text{A5})$$

Equation (A4) is solved by marching forward in time given an initial condition and the spectral wave forcing $U_{\infty,w}(t)$ output from the WAFO toolbox. The resulting in-canopy velocity time series $\hat{U}_w(t)$ for the spectral wave condition is used to calculate the in-canopy wave energy spectrum \hat{S}_U , enabling $\alpha_{w,j}$ to be calculated from equation (8).

Appendix B: Dissipation of Monochromatic Wave Energy by Submerged Canopies

[35] The dissipation of wave energy by a canopy can be calculated from the integral form of the conservation of mechanical energy equation, expressed in indicial notation

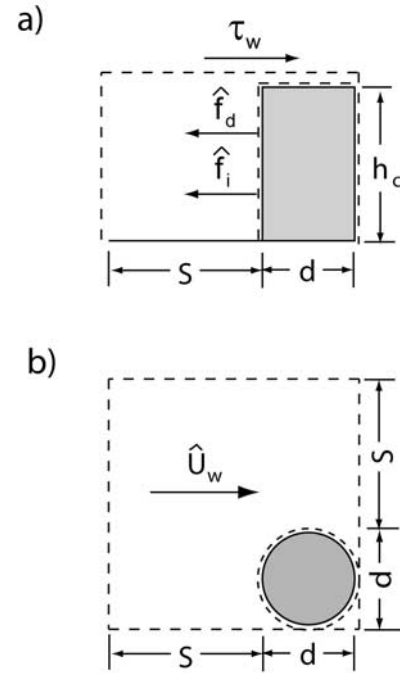


Figure B1. Control volume (indicated by the dashed line) used to calculate dissipation within the canopy, which represents a repeating canopy element unit of plan area $A_T = (S + d)^2$. (a) Section view. (b) Plan view.

where repeated indices imply summation [Kundu and Cohen, 2002],

$$\frac{d}{dt} \int_I E dV + \int_{II} E U_i dA_i = \int_{III} \rho g_i U_i dV + \int_{IV} U_i \tau_{ik} dA_k - \int_V \phi_V dV. \quad (\text{B1})$$

Here $E \equiv \rho U_i U_i / 2$ is the kinetic energy (KE) per unit volume, τ_{ik} is the stress (normal or shear) acting on the control surface area dA_k , and ϕ_V is the rate of viscous dissipation per unit fluid volume. Physically, term I represents the rate of change of KE within the control volume, term II represents the rate of outflow of KE across the control surfaces, term III is the rate of work done by the gravitational body force, term IV represents the rate of work done by surface forces, and term V is the rate of dissipation of KE within the control volume. To determine the rate of dissipation within a canopy, a control volume (Figure B1) can be defined that incorporates a repeating canopy element unit (in this case a single cylinder), and equation (B1) can be used to calculate the rate of dissipation inside. Note that this control volume does not incorporate the volume occupied by the solid cylinder and hence occupies the fluid volume $A_T h_c (1 - \lambda_p)$.

[36] To apply equation (B1), the velocity within and above the canopy must be known. For monochromatic waves, we assume that the velocity above the canopy $U_{\infty,w}(t)$ is defined according to equation (6) and within the canopy is defined by a single representative value $\hat{U}_w(t)$. As discussed in LKM, $\hat{U}_w(t)$ may not be perfectly sinusoidal owing to the nonlinear canopy resistance terms (e.g., owing to the drag and shear stress terms). However, for

simplicity, we assume that it can be approximated by a sinusoidal function in phase with the above-canopy flow; that is,

$$\widehat{U}_w(t) = \alpha_w U_{\infty,w}^{\max} \cos\left(\frac{2\pi t}{T}\right). \quad (\text{B2})$$

In equation (17), ε is defined as the rate of energy dissipation per unit plan area averaged over a period T , while ϕ_V in equation (B1) represents the instantaneous rate of dissipation per unit fluid volume. Therefore ε is simply equal to term V in equation (B1), averaged over a wave period and divided by the plan area of the repeating canopy element unit A_T ; that is,

$$\varepsilon = \frac{1}{A_T} \overline{\int \phi_V dV}, \quad (\text{B3})$$

where the overbar denotes temporal averaging over a wave period. Dissipation ε is then determined by averaging terms I through IV in equation (B1) over a wave cycle and dividing by A_T . It can be shown that, on the basis of equation (B2), terms I through III averaged over a period are each zero. Equation (B1) reduces to

$$\varepsilon = \frac{1}{A_T} \overline{\int \phi_V dV} = \frac{1}{A_T} \overline{\int U_i \tau_{ik} dA_k}, \quad (\text{B4})$$

which shows that the rate of dissipation is equal to the rate of work done by the flow against the forces acting on the control surface.

[37] As discussed in LKM, three forces act on the control surface: (1) a shear stress which acts at the top of the canopy, (2) a drag force exerted by the canopy elements, and (3) an inertial force also exerted by the canopy elements. To evaluate equation (B4) these forces must be quantified, which were parameterized in LKM during the development of equation (1). The total rate of dissipation within the canopy ε can then be decomposed as

$$\varepsilon = \varepsilon_s + \varepsilon_d + \varepsilon_i, \quad (\text{B5})$$

where ε_s , ε_d , and ε_i are the shear, drag, and inertial force contributions, respectively. The shear stress at the top of the canopy was parameterized in equation (14) of LKM using a quadratic friction law; hence

$$\varepsilon_s = \overline{\tau_w U_{\infty,w}} = \frac{2}{3\pi} \rho C_f \left(U_{\infty,w}^{\max} \right)^3. \quad (\text{B6})$$

Similarly, the drag contribution can be determined from the quadratic drag law in equation (16) of LKM; that is,

$$\varepsilon_d = \rho h_c (1 - \lambda_p) \overline{\widehat{f}_d \widehat{U}_w} = \frac{2}{3\pi} \rho C_d \lambda_f \alpha_w^3 \left(U_{\infty,w}^{\max} \right)^3, \quad (\text{B7})$$

where \widehat{f}_d is the canopy drag force per unit canopy fluid. Finally, the inertial force contribution can be calculated from equation (17) of LKM as

$$\varepsilon_i = \rho h_c (1 - \lambda_p) \overline{\widehat{f}_i \widehat{U}_w} = 0, \quad (\text{B8})$$

where \widehat{f}_i is the canopy inertial force per unit canopy fluid mass (defined in equation (17) in LKM). Given that \widehat{f}_i is proportional to $d\widehat{U}_w/dt$ (and hence is 90 degrees out of phase with \widehat{U}_w), the inertial force will not directly contribute to wave energy dissipation. However, the inertial force cannot altogether be neglected since, from equation (1) it will serve to reduce \widehat{U}_w (or α_w), and per equation (B7) will thus indirectly influence the rate at which energy is dissipated by drag.

Appendix C: Dissipation of Spectral Wave Energy by Submerged Canopies

[38] In Appendix B, dissipation of wave energy by a submerged canopy was shown to be equal to the rate of work done by the flow against canopy forces, namely shear, drag and inertial. *Madsen et al.* [1988] (later modified by *Madsen* [1994]) derived a spectral dissipation model by specifically calculating the work done by an oscillatory flow against shear stresses exerted by a bed. We now apply ideas developed in their work to decompose spectral wave energy dissipation by a canopy into both a shear and drag contribution.

[39] *Hasselmann and Collins* [1968] first developed an analytical model to predict how frictional dissipation rates vary among different spectral components by directly evaluating $\overline{\tau_w U_{\infty,w}}$, where they assumed a quadratic form for the shear stress, that is, $\tau_w = \frac{1}{2} \rho C_f |U_{\infty,w}| U_{\infty,w}$, and treated $U_{\infty,w}$ as a random variable. However, the dissipation function they developed included a complex nonlinear interaction term that limited its practical use. Therefore *Collins* [1972] proposed a simplified version, by linearizing τ_w using a velocity ‘‘representative’’ of the spectral wave field $U_{\infty,w}^R$; later *Madsen et al.* [1988] incorporated this representative velocity concept into their spectral dissipation model. Under this assumption, the unsteady shear stress $\tau_{w,j}$ of frequency component j can be expressed as (see equation (26) of *Madsen et al.* [1988]),

$$\tau_{w,j}(t) = \frac{1}{2} \rho C_f U_{\infty,w}^R U_{\infty,j} \cos(\omega_j t), \quad (\text{C1})$$

where for our canopy flow case C_f is the canopy friction coefficient. From equation (B6), the rate of dissipation by shear stresses at the top of the canopy $\varepsilon_{s,j}$ for wave component j is

$$\varepsilon_{s,j} = \overline{\tau_{w,j}(t) U_{\infty,j} \cos(\omega_j t)} = \frac{1}{4} \rho C_f U_{\infty,w}^R U_{\infty,j}^2 \quad (\text{C2})$$

which is identical to equation (26) of *Madsen et al.* [1988]. Note that equation (C2) assumes that the shear stress is in phase with the near-bottom velocity, which was also assumed by *Madsen et al.* [1988]. However, *Madsen* [1994] showed that this phase difference θ_j for each component j introduces a factor $\cos(\theta_j)$ into equation (C2), which will slightly reduce dissipation. This effect is neglected, however, given that a typical maximum value for θ_j is generally assumed to be 30° [*Madsen*, 1994], which introduces at most a $\sim 10\%$ error in $\varepsilon_{s,j}$ among the frequency components.

[40] Up to this point, the analysis exactly follows *Madsen et al.* [1988]. However, on the basis of equations (B4) and (B5) in Appendix B, for a canopy the contributions of drag and inertial forces must also be considered. Analogous to the monochromatic wave case, for spectral waves it can also be shown that dissipation by inertial forces will be zero since this force will be 90 degrees out of phase with the local velocity. Dissipation by canopy drag can be calculated following the same approach that was used above for the shear contribution, since the canopy drag force is governed by the same quadratic law (see equation (1)). From equation (C1), the canopy drag force per unit canopy fluid mass \hat{f}_d given by equation (16) in LKM) can be linearized using the representative velocity concept; that is,

$$\hat{f}_{d,j}(t) = \frac{C_d \lambda_f}{2h_c(1 - \lambda_p)} \widehat{U}_w^R \widehat{U}_j \cos(\omega_j t), \quad (C3)$$

where \widehat{U}_j is the in-canopy velocity of component j , and \widehat{U}_w^R is a representative velocity equivalent to the rms in-canopy wave velocity \widehat{U}_w^{rms} . Note that to predict the spectral distribution of drag forces on a cylinder, *Borgman* [1967] similarly linearized the force of component j using a representative, rms wave velocity. Following equation (B7), the rate of dissipation by canopy drag forces $\varepsilon_{d,j}$ is

$$\varepsilon_{d,j} = \rho h_c (1 - \lambda_p) \overline{\widehat{f}_{d,j}(t) \widehat{U}_j \cos(\omega_j t)} = \frac{1}{4} \rho C_d \lambda_f \widehat{U}_w^R \widehat{U}_j^2. \quad (C4)$$

Equation (C4) is very similar to equation (C2), except dissipation by drag in this case is parameterized in terms of the in-canopy flow. The goal of the analysis, however, is to relate $\varepsilon_{d,j}$ to the above-canopy flow field. Equation (8) showed that the in-canopy flow is related to the above-canopy flow through the attenuation parameter $\alpha_{w,j}$, such that $\widehat{U}_j = \alpha_{w,j} U_{\infty,j}$. Similarly, the representative in-canopy velocity can be related to the representative above-canopy velocity through the use of a representative attenuation parameter α_w^R , defined as

$$\alpha_w^R = \frac{\widehat{U}_w^R}{U_{\infty,w}^R} = \frac{\widehat{U}_w^{rms}}{U_{\infty,w}^{rms}}. \quad (C5)$$

The total rate of dissipation by a canopy $\varepsilon_j = \varepsilon_{s,j} + \varepsilon_{d,j}$ can then be determined using equations (C2) and (C4), leading to

$$\varepsilon_j = \frac{1}{4} \rho \left[C_f + C_d \lambda_f \alpha_w^R \alpha_{w,j}^2 \right] U_{\infty,w}^R U_{\infty,j}^2. \quad (C6)$$

Comparison of equation (24) with equation (C6) shows that the energy dissipation factor $f_{e,j}$ is governed by a simple expression governed by properties of the canopy and the in-canopy flow,

$$f_{e,j} = C_f + C_d \lambda_f \alpha_w^R \alpha_{w,j}^2. \quad (C7)$$

Notation

A_f canopy element frontal area.
 A_p canopy element plan area.

A_∞ horizontal wave orbital excursion amplitude.
 C_d canopy drag coefficient.
 C_f canopy friction coefficient.
 C_M canopy inertial force coefficient.
 d cylinder diameter.
 E flow kinetic energy per unit volume.
 f wave frequency.
 f_d drag force per unit canopy fluid mass.
 f_e energy dissipation factor.
 f_i inertial force per unit canopy fluid mass.
 h_c height of the canopy.
 k wave number.
 k_w bottom roughness length scale.
 L_d canopy drag length scale.
 L_s canopy shear length scale.
 P pressure field.
 S cylinder spacing.
 S_A wave orbital excursion spectrum.
 S_u spectrum based on raw measured velocity time series.
 S_u' turbulent contribution to S_u .
 S_U wave spectrum above canopy.
 \hat{S}_U wave spectrum inside canopy.
 t time.
 T wave period.
 T_p peak wave period.
 u instantaneous velocity in x direction.
 U_c time-averaged current velocity.
 U_w phase-varying wave velocity.
 \widehat{U}_w spatially averaged wave velocity inside the canopy.
 $U_{\infty,w}$ free-stream wave velocity.
 z vertical elevation measured from the canopy base.
 α_c unidirectional canopy flow attenuation parameter.
 α_i attenuation for inertial dominated flow.
 α_w wave canopy flow attenuation parameter.
 Δf_b discrete frequency bandwidth.
 ε dissipation per unit plan area.
 ϕ linear wave decay correction parameter.
 ϕ_V dissipation per unit fluid volume.
 λ_f frontal area canopy geometry parameter.
 λ_p plan area canopy geometry parameter.
 θ_j phase difference between velocity and shear stress for component j .
 ρ fluid density.
 τ canopy shear stress.
 ω radian wave frequency.

Subscripts

c parameter associated with current.
 j discrete frequency component j .
 w parameter associated with waves.

Superscripts

max velocity amplitude.
 R representative value.
 rms root mean squared value.
 ' turbulent contribution.

Other

^ overhat canopy-averaged value.
 - overbar denoting time average operator.
 || absolute value.

[41] **Acknowledgments.** We thank Dan Schar and Nicole Jones for assisting with the field experiment. This work was supported by the National Science Foundation under grant OCE-0117859.

References

- Ardhuin, F., T. H. C. Herbers, and W. C. O'Reilly (2001), A hybrid Eulerian-Lagrangian model for spectral wave evolution with application to bottom friction on the continental shelf, *J. Phys. Oceanogr.*, *31*, 1498–1516.
- Benilov, A. Y., and B. N. Filyushkin (1970), Application of methods of linear filtration to an analysis of fluctuations in the surface layer of the sea, *Izv. Acad. Sci. USSR Atmos. Oceanic Phys. Engl. Transl.*, *6*(8), 810–819.
- Borgman, L. E. (1967), Spectral analysis of ocean wave forces on piling, *J. Waterw. Harbors Coastal Eng. Div. Am. Soc. Civ. Eng.*, *93*, 129–156.
- Brodtkorb, P. A., P. Johannesson, G. Lindgren, I. Rychlik, J. Ryden, and E. Sjo (2000), WAFO: A Matlab toolbox for analysis of random waves and loads, paper presented at 10th International Offshore and Polar Engineering Conference, Int. Soc. of Offshore and Polar Eng., Seattle, Wash. (Available at <http://www.maths.lth.se/matstat/wafo/>)
- Coceal, O., and S. E. Belcher (2005), Mean winds through an inhomogeneous urban canopy, *Boundary Layer Meteorol.*, *115*, 47–68.
- Collins, J. I. (1972), Prediction of shallow-water spectra, *J. Geophys. Res.*, *77*, 2693–2707.
- Dalrymple, R. A., J. T. Kirby, and P. A. Hwang (1984), Wave diffraction due to areas of energy dissipation, *J. Waterw. Port Coastal Ocean Eng.*, *110*, 67–79.
- Dean, R. G., and R. A. Dalrymple (1991), *Water Wave Mechanics for Engineers and Scientists*, 353 pp., World Sci., Hackensack, N. J.
- Denny, M., and B. Gaylord (2002), The mechanics of wave-swept algae, *J. Exp. Biol.*, *205*, 1355–1362.
- Dronkers, J. J. (1964), *Tidal Computations in Rivers and Coastal Waters*, Elsevier, New York.
- Dubi, A., and A. Torum (1997), Wave energy dissipation in kelp vegetation, paper presented at Twenty-Fifth Coastal Engineering Conference, Am. Soc. of Civ. Eng., Orlando, Fla.
- Falter, J. L., M. J. Atkinson, and M. A. Merrifield (2004), Mass transfer limitation of nutrient uptake by a wave-dominated reef flat community, *Limnol. Oceanogr.*, *49*, 1820–1831.
- Gerritsen, F. (1981), Wave attenuation and wave set-up on a coastal reef, paper presented at 17th Coastal Engineering Conference, Am. Soc. of Civ. Eng., Sydney.
- Ghisalberti, M., and H. M. Nepf (2004), The limited growth of vegetated shear flows, *Water Resour. Res.*, *40*, W07502, doi:10.1029/2003WR002776.
- Hasselmann, K., and J. I. Collins (1968), Spectral dissipation of finite-depth gravity waves due to turbulent bottom, *J. Mar. Res.*, *26*, 1–12.
- Jonsson, I. G. (1966), Wave boundary layers and friction factors, paper presented at Tenth Conference on Coastal Engineering, Am. Soc. of Civ. Eng., Tokyo.
- Kajiura, K. (1968), A model of the bottom boundary layer in water waves, *Bull. Earthquake Res. Inst. Univ. Tokyo*, *46*, 75–126.
- Kundu, P. K., and I. M. Cohen (2002), *Fluid Mechanics*, 2nd ed., 730 pp., Elsevier, New York.
- Lowe, R. J., J. L. Falter, M. D. Bandet, G. Pawlak, M. J. Atkinson, S. G. Monismith, and J. R. Koseff (2005a), Spectral wave dissipation on a barrier reef, *J. Geophys. Res.*, *110*, C04001, doi:10.1029/2004JC002711.
- Lowe, R. J., J. R. Koseff, and S. G. Monismith (2005b), Oscillatory flow through submerged canopies: 1. Velocity structure, *J. Geophys. Res.*, *110*, C10016, doi:10.1029/2004JC002788.
- Madsen, O. S. (1994), Spectral wave-current bottom boundary layer flows, paper presented at 24th Coastal Engineering Conference, Am. Soc. of Civ. Eng., Kobe, Japan.
- Madsen, O. S., Y.-K. Poon, and H. C. Graber (1988), Spectral wave attenuation by bottom friction: Theory, paper presented at 21st Coastal Engineering Conference, Am. Soc. of Civ. Eng.
- Massel, S. R. (1996), *Ocean Surface Waves: Their Physics and Prediction*, 491 pp., World Sci., Hackensack, N. J.
- Mathisen, P. P., and O. S. Madsen (1999), Waves and currents over a fixed rippled bed: 3. Bottom and apparent roughness for spectral waves and currents, *J. Geophys. Res.*, *104*, 18,447–18,461.
- Mendez, F. J., and I. J. Losada (2004), An empirical model to estimate the propagation of random breaking and nonbreaking waves over vegetation fields, *Coastal Eng.*, *51*, 103–118.
- Nelson, R. C. (1996), Hydraulic roughness of coral reef platforms, *Appl. Ocean Res.*, *18*, 265–274.
- Nielsen, P. (1992), *Coastal Bottom Boundary Layers and Sediment Transport*, 324 pp., World Sci., Hackensack, N. J.
- Swart, D. H. (1974), Offshore sediment transport and equilibrium beach profiles, *Publ. 131*, Delft Hydraulic Lab., Delft, Netherlands.
- Trowbridge, J., and O. S. Madsen (1984), Turbulent wave boundary-layers. 1: Model formulation and first-order solution, *J. Geophys. Res.*, *89*(C5), 7989–7997.

M. J. Atkinson and J. L. Falter, Hawaii Institute of Marine Biology, University of Hawaii, Kaneohe, HI 96744, USA.

J. R. Koseff and S. G. Monismith, Environmental Fluid Mechanics Laboratory, Department of Civil and Environmental Engineering, Stanford University, Stanford, CA 94305, USA.

R. Lowe, School of Environmental Systems Engineering, University of Western Australia, M015-35 Stirling Highway, Crawley, WA 6009, Australia. (ryan.lowe@uwa.edu.au)